# Comparison of distances for supervised segmentation of white matter tractography

Emanuele Olivetti, Giulia Bertò, Pietro Gori, Nusrat Sharmin, Paolo Avesani

# Comparison of Distances for Supervised Segmentation of White Matter Tractography

Emanuele Olivetti*†, Giulia Bertò*†, Pietro Gori‡, Nusrat Sharmin*† and Paolo Avesani*†
*NeuroInformatics Laboratory (NILab), Bruno Kessler Foundation, Trento, Italy
†Centro Interdipartimentale Mente e Cervello (CIMeC), University of Trento, Italy
‡Image processing and understanding (TII) group, Télécom ParisTech, France

***Abstract*—Tractograms are mathematical representations of the main paths of axons within the white matter of the brain, from diffusion MRI data. Such representations are in the form of polylines, called streamlines, and one streamline approximates the common path of tens of thousands of axons. The analysis of tractograms is a task of interest in multiple fields, like neurosurgery and neurology. A basic building block of many pipelines of analysis is the definition of a distance function between streamlines. Multiple distance functions have been proposed in the literature, and different authors use different distances, usually without a specific reason other than invoking the "common practice". To this end, in this work we want to test such common practices, in order to obtain factual reasons for choosing one distance over another. For these reason, in this work we compare many streamline distance functions available in the literature. We focus on the common task of automatic bundle segmentation and we adopt the recent approach of supervised segmentation from expert-based examples. Using the HCP dataset, we compare several distances obtaining guidelines on the choice of which distance function one should use for supervised bundle segmentation.**

***Index Terms*—diffusion MRI ; tractography ; streamline distances ; supervised segmentation**

## I. Introduction

Current diffusion magnetic resonance imaging (dMRI) techniques, together with tractography algorithms, allow the in-vivo reconstruction of the main white matter pathways of the brain at the millimiter scale, see [1]. The most common representation of the white matter is in terms of 3D polylines, called *streamlines*, where one streamline approximates the path of tens of thousands of axons sharing a similar path. The whole set of streamlines of a brain is called *tractogram* and it is usually composed of $10^5 - 10^6$ streamlines.

In multiple applications, like neurosurgical planning and the study of neurological disorders, tractograms are manipulated by algorithms to support navigation, quantification and virtual dissection, performed by experts, see [2]. During the virtual dissection of a tractogram, a given anatomical bundle of interest is segmented by identifying the streamlines that approximate it best. Such segmentation can be manual, e.g. by manually defining regions of interest (ROIs) crossed by those streamlines, or fully automated, like in the case of unsupervised clustering [3] or supervised segmentation [4], [5].

The research was funded by the Autonomous Province of Trento, Call "Grandi Progetti 2012", project "Characterizing and improving brain mechanisms of attention - ATTEND".

A common basic building block for such algorithms is the definition of a streamline-streamline distance function, to quantify the relative displacements between streamlines. The idea is that streamlines belonging to the same anatomical structure lie at small distances, while streamlines belonging to different anatomical structures lie at greater distances. The specific distance function defines the result of nearest neighbor algorithm applied to a streamline. Such algorithm is used in supervised bundle segmentation, see [4], where an example bundle of a subject is provided in order to learn how to segment the same bundle in the tractogram of another subject.

In the literature, several streamline-streamline distance functions have been proposed. The most common distances rely on streamlines parametrized as sequences of 3D points, even though other parametrizations exist such as B-splines [6] or Fourier descriptors [7]. This kind of distances can then be separated into two main groups: those based on a point-to-point correspondence between streamlines, i.e. minimum-average direct flip (MDF) [8], and those not requiring that (i.e. Hausdorff, currents [9]).

Even though each group of distances has a distinct technical motivation, little has been said to guide the choice of the practitioner when choosing a distance for a specific task. To the best of our knowledge, only in the case of unsupervised bundle segmentation, by means of clustering, some results are available about comparing distances. In [10], four different distances were compared to see the impact on various indexes for clustering of streamlines. In [11], for the task of clustering of streamlines, three distances have been compared, obtaining some evidence that the point density model (PDM) distance should be preferred for that task.

In this work, we propose to address the gap in the literature by providing guidelines for the choice of the streamline-streamline distance function for the specific task of supervised bundle segmentation. Following the ideas in [4], [5], [12], we adopt the supervised segmentation framework, where the desired bundle is automatically segmented from a tractogram starting from an example of that bundle segmented by an expert on a different subject.

We computed the supervised segmentations of 9 bundles with the nearest neighbor algorithm using 8 different distance functions. We compared the obtained bundles first against a ground truth, and then one against each other.

Our results show that the quality of segmented bundles does not significantly change when changing the distance function,

despite the large differences in computational cost. At the same time, we observe that, at the streamline level, different distances result in a different nearest neighbor.

In the following, we first briefly introduce the notation, the streamline distances and the the approximate nearest neighbor algorithms used in this work. In Section III, we describe the details of the experimental setup and provide the results. In Section IV, we discuss the results and draw the conclusions.

## II. Methods

Let $s = \{\mathbf{x}_1, \ldots, \mathbf{x}_n\}$ be a streamline, i.e. a sequence of points, where $\mathbf{x}_i = [x_i, y_i, z_i] \in \mathbb{R}^3, \forall i$. Let $T = \{s_1, \ldots, s_N\}$ be a tractogram and let $b \subset T$ represent the set of streamlines corresponding to an anatomical bundle of interest, e.g. the arcuate fasciculus. Usually, $n$ differs from streamline to streamline, assuming values in the order of $10^1 - 10^2$. We indicate the number of points of a streamline $s$ with $|s|$. $N$ is usually in the order to $10^5 - 10^6$, depending on the parameters of acquisistion of dMRI data and on reconstruction/tracking algorithms.

### A. Streamline distances

Here we define the streamline distances that are frequently used in the literature and that are compared in this work.

- Mean of closest distances [15]:

$$d_{MC}(s_a, s_b) = \frac{d_m(s_a, s_b) + d_m(s_b, s_a)}{2} \tag{1}$$

  where $d_m(s_a, s_b) = \frac{1}{|s_a|} \sum_{\mathbf{x}_i \in s_a} \min_{\mathbf{x}_j \in s_b} ||\mathbf{x}_i - \mathbf{x}_j||_2$
- Shorter mean of closest distances [15]:

$$d_{\text{SC}}(s_a, s_b) = \min(d_m(s_a, s_b), d_m(s_b, s_a)) \tag{2}$$

- Longer mean of closest distances [15]:

$$d_{LC}(s_a, s_b) = \max(d_m(s_a, s_b), d_m(s_b, s_a)) \tag{3}$$

- After re-sampling each streamline to a given number of points $m$, such as $s_a = \{\mathbf{x}_1^a, \ldots, \mathbf{x}_m^a\}$ and $s_b = \{\mathbf{x}_1^b, \ldots, \mathbf{x}_m^b\}$, the MDF distance, see [8] is defined as:

$$d_{\text{MDF},m}(s_a, s_b) = \min(d_{\text{direct}}(s_a, s_b), d_{\text{flipped}}(s_a, s_b)) \tag{4}$$

  where $d_{\text{direct}}(s_a, s_b) = \frac{1}{m} \sum_{i=1}^{m} ||\mathbf{x}_i^a - \mathbf{x}_i^b||_2$ and $d_{\text{flipped}}(s_a, s_b) = \frac{1}{m} \sum_{i=1}^{m} ||\mathbf{x}_i^a - \mathbf{x}_{m-i+1}^b||_2$
- Point Density Model (PDM, see [11]):

$$d^2_{\text{PDM}}(s_a, s_b) = \langle s_a, s_a \rangle_{pdm} + \langle s_b, s_b \rangle_{pdm} - 2\langle s_a, s_b \rangle_{pdm} \tag{5}$$

  where

$$\langle s_a, s_b \rangle_{pdm} = \frac{1}{|s_a||s_b|} \sum_{i=1}^{|s_a|} \sum_{j=1}^{|s_b|} K_\sigma(\mathbf{x}_i^a, \mathbf{x}_j^b) \tag{6}$$

  and $K_\sigma(\mathbf{x}_i^a, \mathbf{x}_j^b) = \exp\left(-\frac{||\mathbf{x}_i^a - \mathbf{x}_j^b||_2^2}{\sigma^2}\right)$ is a Gaussian kernel between the two 3D points.
- Varifolds distance (see [16]) is the non-oriented version of the currents [9] distance, namely it does not need streamlines $a$ and $b$ to have a consistent orientation.

$$d^2_{\text{varifolds}}(s_a, s_b) = \langle s_a, s_a \rangle_{var} + \langle s_b, s_b \rangle_{var} - 2\langle s_a, s_b \rangle_{var} \tag{7}$$

  where

$$\langle s_a, s_b \rangle_{var} = \sum_{i=1}^{|s_a|-1} \sum_{j=1}^{|s_b|-1} K_\sigma(\mathbf{p}_i^a, \mathbf{p}_j^b) K_n(\mathbf{n}_i^a, \mathbf{n}_j^b) |\mathbf{n}_i^a|_2 |\mathbf{n}_j^b|_2 \tag{8}$$

  with $K_n(\mathbf{n}_i^a, \mathbf{n}_j^b) = \left(\frac{(\mathbf{n}_i^a)^T \mathbf{n}_j^b}{|\mathbf{n}_i^a|_2 |\mathbf{n}_j^b|_2}\right)^2$ where $\mathbf{p}_i^a$ (resp. $\mathbf{p}_j^b$) and $\mathbf{n}_i^a$ (resp. $\mathbf{n}_j^b$) are the center and tangent vector of segment $i$ (resp. $j$) of streamline $a$ (resp. $b$). The endpoints of segment $i$ are $\mathbf{x}_i$ and $\mathbf{x}_{i+1}$ for $i \in [1, ..., n-1]$.

### B. Supervised Segmentation of Bundles

As in [4], [5], we segment a bundle of interest in the tractogram of a given (target) subject using a supervised procedure. This means that we leverage the segmentation of the same bundle in the tractogram of another subject, as an example. Assuming that the tractograms of the two subjects are registered in the same space, e.g. see [8], a simple supervised segmentation method is based on the nearest neighbor algorithm: we define the segmented bundle as the set of streamlines of the target subject that are nearest neighbor of the streamlines of the example bundle.

More formally, let $T^A_{\text{example}}$ and $T^B_{\text{target}}$ be the tractograms of two different subjects, $A$ and $B$. Let $b^A_{\text{example}} \subset T^A_{\text{example}}$ be an example of the bundle of interest, segmented by an expert. Let $b^B_{\text{target}} \subset T^B_{\text{target}}$ be the (unknown) corresponding bundle we want to approximate using automatic supervised segmentation, via nearest neighbor. Under the assumptions that $T^A_{\text{example}}$ and $T^B_{\text{target}}$ are co-registered, the approximate bundle $\hat{b}^B_{\text{target}} \subset T^B_{\text{target}}$ is such that

$$\hat{b}^B_{\text{target}} = \{\text{NN}(s_e^A, T^B_{\text{target}}), \forall s_e^A \in b^A_{\text{example}}\} \tag{9}$$

where $s_e^A$ is a streamline of the example tract of subject $A$ and $\text{NN}(s_e^A, T^B_{\text{target}}) = \text{argmin}_{s^B \in T^B_{\text{target}}} d(s_e^A, s^B)$ its nearest neighbor streamline in $T^B_{\text{target}}$, i.e. the one having minimum distance from $s_e^A$.

The notion of streamline-streamline distance can be implemented in multiple ways, such as those listed above, in Section II-A. For this reason, different distances induce different segmentations.

Notice that, in principle, computing the nearest neighbors of the streamlines in $T^B_{\text{target}}$ is expensive, in terms of computations. The most basic algorithm would require the computation of $|b^A_{\text{example}}| \times |T^B_{\text{target}}|$ distances, which is usually in the order of $10^7 - 10^9$. According to the timings in Table II, a single nearest neighbors segmentation may require over 24 hours of computation, in case of a large bundle.

### C. Efficient Computation of Nearest Neighbor

Based on the results in [17], we adopt a simple procedure to efficiently compute the approximate nearest neighbor of a streamline, that reduces the amount of computations of several orders of magnitudes with respect to the standard algorithm. The procedure is the following: first, we transform each streamline in $T_{\text{target}}$ into an $d$-dimensional vector, using an Euclidean embedding technique called *dissimilarity representation* [18]. For lack of space, we refer the reader

to [17] for all the details. Second, we put all vectors in a $k$-d tree [19], which is a space partitioning data structure that provides efficient 1-nearest neighbor search, which requires only $\mathcal{O}(\log N)$ steps, $N = |T_{\text{target}}|$. Then, for each streamline in $b_{\text{example}}$, we transform it into a vector using again the dissimilarity representation step above and we compute its nearest neighbor in $T_{\text{target}}$ through the $k$-d tree.

## III. Experiments

We conducted multiple experiments on the the Human Connectome Project (HCP) dMRI datasets, see [13], [20], (90 gradients; b = 1000; voxel size = (1.25 x 1.25 x 1.25 $mm^3$)). The reconstruction step was performed using the constrained spherical deconvolution (CSD) algorithm [21] and the tracking step using the Euler Delta Crossing (EuDX) algorithm [3] with $10^6$ seeds. We adopted the white matter query language (WMQL) [14] to obtain 9 segmented bundles for 10 random subjects, which we considered as ground truth. We selected the bundles reproducing the selection in [12], where they aimed to avoid extreme variability of the same bundle across subjects, due to the limitations of WMQL. The selected bundles are reported in the first column of Table I. Each pair of tractograms was co-registered using the streamline linear registration (SLR) algorithm [8].

As explained in Section II-C, we represented the streamlines into a vectorial space, in order to obtain fast nearest neighbor queries. We considered 8 different distance functions, described in Section II: $d_{\text{MC}}$, $d_{\text{SC}}$, $d_{\text{LC}}$, $d_{\text{MDF,12}}$, $d_{\text{MDF,20}}$, $d_{\text{MDF,32}}$, $d_{\text{PDM}}$ and $d_{\text{varifolds}}$. For $d_{\text{PDM}}$ and $d_{\text{varifolds}}$ we set $\sigma = 42mm$, according to [11]. For each subject and distance function, we computed the dissimilarity representation of the (target) tractogram $T^B_{\text{target}}$. According to [17], we selected 40 prototypes with the subset farthest first (SFF) policy. Then we built the $k$-d tree of each $T^B_{\text{target}}$. For each possible example bundle $b^A_{\text{example}}$, we first computed its dissimilarity representation with the prototypes of $T^B_{\text{target}}$, then segmented the target bundle $\hat{b}^B_{\text{target}}$ by querying the $k$-d tree.

Following the common practice, see [8], as accuracy of the estimation, we measured the degree of overlap between $\hat{b}^B_{\text{target}}$ and the true target bundle $b^B_{\text{target}}$, through the dice similarity coefficient (DSC) at the voxel-level: $DSC = 2\frac{|v(\hat{b}^B_{\text{target}}) \cap v(b^B_{\text{target}})|}{|v(\hat{b}^B_{\text{target}})| + |v(b^B_{\text{target}})|}$ where $v(b)$ is the set of voxels crossed by the streamlines of bundle $b$ and $|v(b)|$ is the number of voxels of $v(b)$.

The experiments were developed in Python code, on top of DiPy[1]. The code of all experiments is available under a Free/OpenSource license at http://github.com/emanuele/prni2017_comparison_of_distances.

### A. Results

In Table I, we report the degree of overlap, as mean DSC, obtained with the nearest neighbor supervised segmentation, across the different tracts and the 8 different distance functions considered. The mean is computed over all 90 pairs $(b^A_{\text{example}}, T^B_{\text{target}})$, obtained from the 10 subjects. For each bundle and distance function, we observed a standard deviation of DSC of approximately $0.10$ [2]. Such value includes the variances due to: the anatomical variability across subjects, the limitations of the WMQL segmentation used as ground truth and, in minor part, the approximation introduced by the dissimilarity representation[3].

TABLE I
Mean DSC voxel table

| | $d_{\text{MC}}$ | $d_{\text{SC}}$ | $d_{\text{LC}}$ | $d_{\text{MDF,12}}$ | $d_{\text{MDF,20}}$ | $d_{\text{MDF,32}}$ | $d_{\text{PDM}}$ | $d_{\text{varifolds}}$ |
|---|---|---|---|---|---|---|---|---|
| cg.left | 0.61 | 0.60 | 0.59 | 0.59 | 0.59 | 0.59 | 0.59 | 0.56 |
| cg.right | 0.60 | 0.59 | 0.58 | 0.58 | 0.57 | 0.58 | 0.57 | 0.55 |
| ifof.left | 0.49 | 0.48 | 0.47 | 0.48 | 0.48 | 0.47 | 0.48 | 0.49 |
| ifof.right | 0.47 | 0.46 | 0.45 | 0.45 | 0.45 | 0.45 | 0.46 | 0.44 |
| uf.left | 0.52 | 0.54 | 0.55 | 0.52 | 0.52 | 0.53 | 0.57 | 0.60 |
| uf.right | 0.49 | 0.52 | 0.51 | 0.49 | 0.49 | 0.49 | 0.52 | 0.56 |
| cc_7 | 0.58 | 0.56 | 0.61 | 0.64 | 0.63 | 0.63 | 0.59 | 0.67 |
| cc_2 | 0.49 | 0.50 | 0.52 | 0.53 | 0.53 | 0.54 | 0.57 | 0.59 |
| af.left | 0.51 | 0.49 | 0.51 | 0.51 | 0.50 | 0.50 | 0.52 | 0.50 |
| **means** | **0.53** | **0.53** | **0.53** | **0.53** | **0.53** | **0.53** | **0.54** | **0.55** |

In Table II, we report the time required by a modern desktop computer to compute 90000 streamline-streamline distances using the 8 distance functions considered in this study. The differences in time are due to both the different computational cost of the formulas in Section II and their implementation. $d_{\text{MC}}$, $d_{\text{SC}}$, $d_{\text{LC}}$ and $d_{\text{MDF}}$, available from DiPy, were implemented in Cython. $d_{\text{PDM}}$ and $d_{\text{varifolds}}$ were implemented by us in Python and NumPy[4].

TABLE II
Computational time for 90000 pairs of streamlines.

| | $d_{\text{MC}}$ | $d_{\text{SC}}$ | $d_{\text{LC}}$ | $d_{\text{MDF,12}}$ | $d_{\text{MDF,20}}$ | $d_{\text{MDF,32}}$ | $d_{\text{PDM}}$ | $d_{\text{varifolds}}$ |
|---|---|---|---|---|---|---|---|---|
| time(s) | 0.5 | 0.5 | 0.5 | 0.03 | 0.04 | 0.05 | 16 | 28 |

In order to collect more insight on the results of Table I, we investigated in Figure 1 whether different distance functions returned the same nearest neighbor streamlines. We expect that distance functions, that are based on different geometric principles, have a different nearest neighbor. In Figure 1, each entry represents the frequency with which two distance functions returned the same nearest neighbor of a given streamline. Such frequency is computed over all streamlines of all tracts of all pairs of subjects considered in the experiments, i.e. approximately 200000 nearest neighbor computations.

## IV. Discussion and Conclusion

The results reported in Table I clearly show that there are no major differences in the accuracy of the supervised segmented bundles, measured as DSC, when using different distance functions. The highest mean DSC value, i.e. $0.55$ for $d_{\text{varifolds}}$, is not significantly higher than the other values. This is partly different from the results reported in [11] but, as mentioned in Section I, that work investigated segmentation as *unsupervised* clustering of streamlines, while we focus on *supervised* bundle segmentation. The supervised approach is example-based, thus directly driven by anatomy, while clustering is not. For this

[1] http://nipy.org/dipy, [22].

[2] Which correspond to a standard deviation of the mean of $0.01$.

[3] Via bootstrap, we estimated an average contribution of $0.015$ to the value of the standard deviation of DSC.

[4] http://www.numpy.org

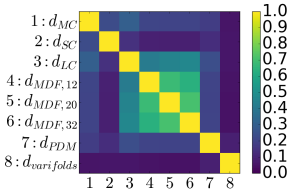


Fig. 1. Frequency with which two distance functions selected the same nearest neighbor of a streamline during all our experiments.

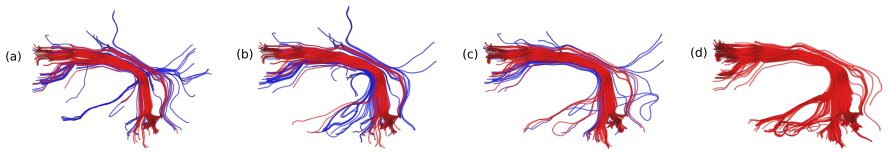


Fig. 2. Example of segmented arcuate fasciculus left with NN using (a) $d_{\text{LC}}$ (DSC=0.64) (b) $d_{\text{MDF,20}}$ (DSC=0.69) and (c) $d_{\text{varifolds}}$ (DSC=0.71). (d) Ground truth arcuate fasciculus left. True positive streamlines in red and false positives in blue. Subject A: HCP ID 201111, subject B: HCP ID 124422.

reason, differences in the results of the two approaches are to be expected.

The results in Figure 1 show that different distance functions often result in different nearest neighbor of a streamline, with some exceptions. Expectedly, all MDF distance functions frequently select the same nearest neighbor, ≈65% of the times. Surprisingly, $d_{\text{LC}}$ agrees with them ≈45% of the times. In all other cases the agreement is very low, between $5\%$ and $25\%$.

Why do different nearest neighbors lead to a similar quality of segmentation? The potential disagreement between the results in Table I and Figure 1 can be explained by the following argument. At the *local* level, different distances clearly have a geometrically different concept of proximity, frequently leading to different nearest neighbors. Nevertheless, we observed that such different neighbors do not lie far apart from each other so, at a *higher/aggregated* level of bundle, it should not be a surprise that they lead to a comparable quality of segmentation. This can also be seen in Figure 2, where the false positives of the bundles segmented with different distances are almost the same, while the false negatives are different. Moreover, Table I presents a *voxel* measure of bundle overlap, while Figure 1 presents a *streamline* measure. A voxel-based measure of bundle overlap is inherently less sensitive than a streamline-based measure, because different proximal streamlines usually have many voxels in common. So when two distance functions lead to different (but proximal) nearest neighbors, they will positively contribute in terms of voxel overlap, but not in terms of streamline overlap.

Furthermore, we observe in Table II that the computational times of the distance functions can be very different. For instance, there are more than two orders of magnitude between the computational time of $d_{\text{MDF}}$ and the one of $d_{\text{varifolds}}$. To conclude, for the supervised segmentation task based on a voxel-based measure, we suggest that practitioners prefer fast distance functions, such as $d_{\text{MDF}}$, $d_{\text{MC}}$, $d_{\text{SC}}$ or $d_{\text{LC}}$, over slower ones, like $d_{\text{PDM}}$ and $d_{\text{varifolds}}$.

## REFERENCES


[1] M. Catani and M. T. de Schotten, *Atlas of Human Brain Connections*, 1st ed. Oxford University Press, Apr. 2015.

[2] M. Catani, R. J. Howard, S. Pajevic, and D. K. Jones, "Virtual in vivo interactive dissection of white matter fasciculi in the human brain." *NeuroImage*, vol. 17, no. 1, pp. 77–94, Sep. 2002.

[3] E. Garyfallidis, M. Brett, M. M. Correia, G. B. Williams, and I. Nimmo-Smith, "QuickBundles, a Method for Tractography Simplification." *Frontiers in neuroscience*, vol. 6, 2012.

[4] S. W. Yoo, P. Guevara, Y. Jeong, K. Yoo, J. S. Shin, J.-F. Mangin, and J.-K. Seong, "An Example-Based Multi-Atlas Approach to Automatic Labeling of White Matter Tracts," *PloS one*, vol. 10, no. 7, 2015.

[5] N. Sharmin, E. Olivetti, and P. Avesani, "Alignment of Tractograms as Linear Assignment Problem," in *Computational Diffusion MRI*. Springer, 2016, pp. 109–120.

[6] I. Corouge, P. Fletcher, S. Joshi, S. Gouttard, and G. Gerig, "Fiber tract-oriented statistics for quantitative diffusion tensor MRI analysis," *Medical Image Analysis*, vol. 10, no. 5, pp. 786–798, Oct. 2006.

[7] P. G. Batchelor, F. Calamante, J. D. Tournier, D. Atkinson, D. L. G. Hill, and A. Connelly, "Quantification of the shape of fiber tracts," *Magnetic Resonance in Medicine*, vol. 55, no. 4, pp. 894–903, Apr. 2006.

[8] E. Garyfallidis, O. Ocegueda, D. Wassermann, and M. Descoteaux, "Robust and efficient linear registration of white-matter fascicles in the space of streamlines," *NeuroImage*, vol. 117, pp. 124–140, Aug. 2015.

[9] P. Gori, O. Colliot, L. Marrakchi-Kacem, Y. Worbe, F. De Vico Fallani, M. Chavez, C. Poupon, A. Hartmann, N. Ayache, and S. Durrleman, "Parsimonious Approximation of Streamline Trajectories in White Matter Fiber Bundles." *IEEE transactions on medical imaging*, Jul. 2016.

[10] B. Moberts, A. Vilanova, and J. J. van Wijk, "Evaluation of Fiber Clustering Methods for Diffusion Tensor Imaging," in *VIS 05. IEEE Visualization, 2005.* IEEE, 2005, pp. 65–72.

[11] V. Siless, S. Medina, G. Varoquaux, and B. Thirion, "A Comparison of Metrics and Algorithms for Fiber Clustering," in *2013 International Workshop on Pattern Recognition in Neuroimaging*. IEEE, Jun. 2013, pp. 190–193.

[12] E. Olivetti, N. Sharmin, and P. Avesani, "Alignment of Tractograms As Graph Matching," *Frontiers in Neuroscience*, vol. 10, 2016.

[13] S. N. Sotiropoulos, S. Moeller, S. Jbabdi, J. Xu, J. L. Andersson, E. J. Auerbach, E. Yacoub, D. Feinberg, K. Setsompop, L. L. Wald, and Others, "Effects of image reconstruction on fiber orientation mapping from multichannel diffusion MRI: reducing the noise floor using SENSE," *Magnetic resonance in medicine*, vol. 70, no. 6, pp. 1682–1689, 2013.

[14] D. Wassermann, N. Makris, Y. Rathi, M. Shenton, R. Kikinis, M. Kubicki, and C.-F. F. Westin, "On describing human white matter anatomy: the white matter query language." *Medical image computing and computer-assisted intervention : MICCAI ... International Conference on Medical Image Computing and Computer-Assisted Intervention*, vol. 16, no. Pt 1, pp. 647–654, 2013.

[15] S. Zhang, S. Correia, and D. H. Laidlaw, "Identifying White-Matter Fiber Bundles in DTI Data Using an Automated Proximity-Based Fiber-Clustering Method," *IEEE Transactions on Visualization and Computer Graphics*, vol. 14, no. 5, pp. 1044–1053, Sep. 2008.

[16] N. Charon and A. Trouvé, "The Varifold Representation of Nonoriented Shapes for Diffeomorphic Registration," *SIAM Journal on Imaging Sciences*, vol. 6, no. 4, pp. 2547–2580, Jan. 2013.

[17] E. Olivetti, T. B. Nguyen, and E. Garyfallidis, "The Approximation of the Dissimilarity Projection," *IEEE Intl Workshop on Pattern Recognition in NeuroImaging*, vol. 0, pp. 85–88, 2012.

[18] E. Pekalska and R. P. W. Duin, *The Dissimilarity Representation for Pattern Recognition: Foundations And Applications (Machine Perception and Artificial Intelligence)*. World Scientific Publishing Company, Dec. 2005.

[19] J. L. Bentley, "Multidimensional binary search trees used for associative searching," *Communications of the ACM*, vol. 18, no. 9, pp. 509–517, 1975.

[20] D. C. Van Essen, S. M. Smith, D. M. Barch, T. E. J. Behrens, E. Yacoub, and K. Ugurbil, "The WU-Minn Human Connectome Project: An overview," *NeuroImage*, vol. 80, pp. 62–79, Oct. 2013.

[21] J.-D. Tournier, F. Calamante, and A. Connelly, "Robust determination of the fibre orientation distribution in diffusion MRI: Non-negativity constrained super-resolved spherical deconvolution," *NeuroImage*, vol. 35, no. 4, pp. 1459–1472, May 2007.

[22] E. Garyfallidis, M. Brett, B. Amirbekian, A. Rokem, S. van der Walt, M. Descoteaux, I. Nimmo-Smith, and D. Contributors, "Dipy, a library for the analysis of diffusion MRI data," *Frontiers in Neuroinformatics*, vol. 8, no. 8, pp. 1+, Feb. 2014.